A synthetic method to assay polycystin channel biophysics.

Megan Larmore[1], Orhi Esarte Palomero[1], Neha P. Kamat[2,3], Paul G. DeCaen[1,3,4]*

1. Department of Pharmacology, Feinberg School of Medicine, Northwestern University, Chicago, Illinois, USA.

2. Department of Biomedical Engineering, McCormick School of Engineering and Applied Science, Northwestern University, Evanston, Illinois, USA.

3. Center for Synthetic Biology, Northwestern University, Evanston, Illinois, USA

4. Chemistry of Life Processes Institute, Northwestern University, Evanston, Illinois, USA

ABSTRACT

Ion channels are biological transistors that control ionic flux across cell membranes to regulate electrical transmission and signal transduction. They are found in all biological membranes and their conductive states are frequently disrupted in human diseases. Organelle ion channels are among the most resistant to functional and pharmacological interrogation. Traditional channel protein reconstitution methods rely upon exogenous expression and/or purification from endogenous cellular sources which are frequently contaminated by resident ionophores. Here we describe a fully synthetic method to assay the functional properties of the polycystin subfamily of transient receptor potential (TRP) channels that natively traffic to primary cilia and endoplasmic reticulum organelles. Using this method, we characterize their membrane integration, orientation and conductance while comparing these results to their endogenous channel properties. Outcomes define a novel synthetic approach that can be applied broadly to investigate other channels resistant to biophysical analysis and pharmacological characterization.

INTRODUCTION

Ion channels are pore forming integral transmembrane proteins essential for all cellular lifeforms[1, 2]. At the plasma membrane, ion channels are responsible for generating long range bioelectric conduction in excitable eukaryotic cells (e.g. neurons), and within prokaryotic colonies (e.g. bacteria biofilms), and filamentous colonies of archaea[3-5]. Here, they contribute to fundamental vital cell processes including division, signal transduction, and ionic homeostasis[1]. In eukaryotic organelle membranes, ion channels are integral to a wide range of functions including energy production (mitochondria), and the maintenance of defining compartmental conditions such as Ca^{2+} gradients (endoplasmic reticulum), pH (lysosome) and redox states (peroxisome)[6-8]. The conductive states of channels are precisely controlled by their molecular conformations which are unique among their phylogenetic families and subfamilies[9]. More than 400 human genes encode ion channel subunits, many of which are altered by variants that impact organ function and development[10-12]. These so called 'Channelopathies' manifest in various human diseases such as cardiac arrhythmias, neurological conditions, and cystic kidney diseases[13, 14]. Besides their association with disease-causing variants, channels are important therapeutic targets for treating various pathophysiologies and represent the second largest target among the existing FDA-approved drug portfolio[15-17]. However, many members of the so called "dark genome" of understudied proteins encode putative ion channels that are implicated in human disease but remain resistant to functional characterization[18]. Furthermore, channels which localize to cellular compartments in low quantities present a significant challenge to assay for drug screening purposes[19]. Thus, these observations warrant the present investigation of a novel methodological approach to characterize ion channel biophysics and pharmacology.

Voltage clamp electrophysiology incarnated in either planar or glass electrode designs provide direct, real-time and the highest available fidelity measurements of the ion channel conductive states. In the on-cell or inside-out configurations, their opening and closing conformational changes (i.e. gating) are captured as stochastic single channel currents after forming high resistance seals (>10 MΩ) at the interface of the electrode against a biological membrane[20]. This conventional electrophysiology technique is commonly used to characterize the properties of plasma membrane channels and typically involves either recording from an endogenous cell source or from a cell line expressing the channel transgene [21, 22]. However, capturing the biophysical properties of organelle channels and those from bacteria can be mired by electrode inaccessibility to inner membranes. As a work around, investigators have employed various channel reconstitution methods which typically consist of several steps[23, 24]. First, the channel of interest is expressed and immunopurified from a biological cell source, then it is reconstituted into a synthetic or into biologically derived lipid bilayers or vesicles. While there are many examples where heterologous approaches have faithfully reproduced the functional properties of channels from native sources, these preparations are frequently contaminated by endogenous ionophores from the host cell lines, even after purification[25, 26].

To address this, we have developed a completely synthetic method to assay ion channel biophysics. The approach combines advances in cell-free protein expression (CFE) and reconstitution of the synthetic channel protein into giant unilamellar vesicles (GUV) where their single channel properties can be measured using voltage-clamp electrophysiology[27-29]. CFE is a form of *in vitro* protein synthesis, utilizing

purified cellular machinery (ribosomes, tRNAs, enzymes, cofactors, etc.) needed to directly transcribe and translate user-supplied DNA plasmid encoding an ion channel. The unmodified channel proteins are reconstituted into GUVs— cell-sized model membrane systems derived from electrolysis of synthetic lipid mixtures. To validate this method, we characterized PKD2 and PKD2L1 channels, two members of the polycystin subfamily of transient receptor potential (TRP) ion channels. Polycystin subunits can form hetero- and homotetrameric ion channel complexes with several members of the TRP family, where they traffic to the primary cilia and ER organelle membranes[30]. Both features present challenges for experimentalist to functionally characterize these channel properties within their endogenous cell membranes. The medical and biological importance of polycystins is underscored by PKD2 variants associated with autosomal dominant polycystic kidney disease (ADPKD), and this channel's role in fertility and conferring right-left symmetry in embryonic development[31-33]. While PKD2L1 variants have yet to be linked to human disease, its loss of expression results in epilepsy susceptibility and autism -like features in mice[34, 35]. In this report, we stepwise express and confirm protein expression of polycystin channels using the CFE method; reconstitute channel protein in GUVs containing distinct lipid components; assess correct membrane orientation using self-labeling saturated N-heterocyclic building blocks (SNAP) protein chemistry and evaluate channel properties using electrophysiology[36]. Outcomes define a novel reductionist and generalizable approach to study ion channels resistant to biophysical characterization.

RESULTS AND DISCUSSION

We began by carrying out CFE in vitro synthesis of PKD2L1 protein in the presence and absence of lipid vesicles. Plasmid DNA encoding human PKD2L1 with C-terminally tagged green fluorescent protein (PKD2L1-GFP) was added to the cell-free expression components (PURExpress, New England Biolabs) and induced protein translation by heat (**Figure 1A**, See methods). Each reaction produced 8 ± 3.5 μg/μl of synthetic channel protein as estimated by a standardized GFP absorbance assay (**Figure 1— figure supplement 1A**). The synthetically derived channel protein identity was confirmed using two methods. First, by western blot of the cell-free reaction where the PKD2L1-GFP protein was SDS-PAGE gel separated from the reactants and detected by an anti-GFP monoclonal antibody (**Figure 1B**). Second, the PKD2L1 protein was confirmed by mass spectroscopy with 46% coverage (**Figure 1— figure supplement 1B,C**). Since polycystins are transmembrane proteins, we hypothesize that channel membrane incorporation would be facilitated by including lipid substrates into the CFE reaction. Thus, we compared channel synthesis in the presence or absence of small unilamellar vesicles (SUVs) comprised of 1,2-diphytanoyl-sn-glycero-phosphocholine (DPhPC; 4ME16:0PC) and cholesterol (**Figure 1A**). We monitored PKD2L1-GFP protein production over time through fluorescence which is dependent on complete channel translation and correct GFP folding[37]. We observed a dramatic increase in fluorescence output which plateaued after 3 hours when CFEs reactions were supplemented with SUVs—and affect not observed in water-supplement (H_2O) control reactions (**Figure 1C**)[38]. Minimal changes in fluorescence detected when a control plasmid (Ctrl) encoding a non-fluorescent protein (dihydrofolate reductase) was used in the reaction. Taken together, these results demonstrate the efficacy of synthesizing full length polycystin channels using the cell free expression system, and the

enhancement of transmembrane protein synthesis through lipid vesicle incorporation during these reactions.

One caveat of membrane protein vesicle reconstitution is the potential for misorientation after integration. To assay channel orientation, we synthesized PKD2L1 with a C-terminal SNAP-tag fusion protein (PKD2L1-SNAP). The SNAP-tag specifically reacts with fluorescent O2-benzylcytosine derivatives and, depending on the membrane permeability, will react with lipid integrated proteins based on the tag's accessibility (**Figure 2— figure supplement 1**). GUVs containing CFE synthesized PKD2L1-SNAP were formed by electroformation after passing current through indium tin oxide slides treated with dried SUV-channel protein mixture[39]. We then added two substrates, membrane permeable SNAP-Cell Oregon Green (Cell488) and membrane impermeable SNAP-Surface Alexa Fluor 647 (Surface647), to monitor orientation-dependent membrane protein reactivity with the SNAP label (**Figure 2A, Figure 2— figure supplement 1**). We hypothesized there will be two fluorescent outcomes. First, if all channels orient correctly, then we should see only Cell488 fluorescence with no Surface647 at the membrane (**Figure 2A**). Second, if the channels are in opposite or in mixed orientations, then we expect to see dual fluorescence of Cell488 and Surface647 (**Figure 2B**). We imaged over 60 GUVs and found 38.5% of the vesicles exhibited sole Cell488 fluorescence— indicating their correct channel orientation within this population (**Figure 2B, C**). Importantly, none of the vesicle membranes labeled with both Cell488 and Surface647 while retaining a clear lumen— suggesting that the population of GUVs containing misoriented channels was nominal. In some cases, vesicles can encapsulate dye through compromised integrity or mechanisms other than membrane permeability. This is apparent when fluorescence can be seen in the vesicle lumen, rather than on the membrane (**Figure 2C**). While the encapsulated fluorescent vesicles account for most of the vesicles imaged, there were no vesicles seen with Cell488 and Surface647 fluorescence at the membrane with a clear lumen (**Figure 2B, C**). Based on these results, we conclude that our cell-free synthesized PKD2L1 channels are successfully reconstituted in GUVs in the correct orientation, and this preparation is suitable assaying PKD2L1 channels using electrophysiology.

Native and transgene expressed PKD2L1 channels conduct monovalent cations, thus we established symmetric potassium ion (K^+) recording conditions to measure synthetic polycystin currents from GUVs. GUVs containing PKD2L1 were voltage-clamped using 4-7 MΩ resistance (R) glass electrodes in the inside-out membrane patch configuration (**Figure 3A**). After obtaining high resistance seals (R >10 GΩ), single channel events were observed in 23% (26/113 GUVs). However, many of these GUV patches were unstable during voltage steps and were excluded from the final analysis. From the stable recordings, two magnitudes of single channels were readily observed from GUVs containing PKD2L1, suggesting unique full and sub-conductance states (**Figure 3B, C**, **Table 1**). In some recordings, only one conductance predominates, which can be estimated from recoding from individual GUVs (**Figure 3— figure supplement 1A, B**). While in other recordings, both full (*FC*) and sub conductive (*SC*) states can be identified by histogram analysis of the unitary current (**Figure 3— figure supplement 1C, D**). Importantly, no single channel events were observed from GUVs (N= 11) derived from CFE reactions with the empty plasmid— indicating that the measured conductance is not due to a contaminates from lipid or cell-free reagents (**Figure 3B**). To assess the selectivity of the synthetic PKD2L1 pore, we substituted the pipette K^+ charge carrier for methyl-D-glucamine ions ($NMDG^+$). We did not observe any outward single channel

152 currents (i.e. towards the bath), indicating the large cation was not permeable through PKD2L1 which is
153 consistent with previous reports (**Figure 3D, E**)[40, 41]. To determine the feasibility of using this approach
154 to assess the function of other polycystin channels, we followed the same steps to assay PKD2 channel
155 biophysics. Single channels were observed more frequently from PKD2 incorporated GUVs (63% or
156 32/49) compared to PKD2L1 GUVs. As observed with PKD2L1 GUVs, the membrane resistance of
157 synthetic PKD2 GUVs were often destabilized by voltage steps. Importantly, this membrane instability
158 was not observed from empty GUV recordings, suggesting that opening of incorporated polycystin
159 channels during voltage transitions is responsible for patch destabilization. As observed in our PKD2L1
160 results, unitary single channel currents of synthetic PKD2 channels reconstituted in GUVs yield sub- and
161 full conductances, which were blocked by substitution of K^+ with $NMDG^+$ in the electrode (**Figure 4A-C**;
162 **Figure 3— figure supplement 1E-H**). To compare the properties of the synthetic and biologically derived
163 channels, we recorded native PKD2L1 and PKD2 channel single channel currents from the primary cilia
164 membranes of hippocampal neurons and inner medullary collecting duct (IMCD) cell line, respectively
165 (**Figure 4—figure supplement 1**)[34, 42, 43]. Like the synthetic PKD2 and PKD2L1 channels, native polycystins
166 produced sub and full K^+ conductances with inward currents having the greater magnitudes. Here, the
167 synthetic PKD2L1 GUV conductance approximates the native full and subconductances recorded from
168 hippocampal primary cilia membranes cultured from neonatal mice (ARL13B-EGFP^{tg}). However, the
169 PKD2 K^+ conductance magnitudes recorded IMCD cilia were significantly larger than those assayed using
170 the CFE-GUV synthetic system (**Table 1**). These differences might arise from the lack of post-translational
171 modifications (e.g. phosphorylation and N-glycosylation) to the synthetic PKD2 peptides, which are
172 normally found in biologically derived channels [44-46]. In addition, the GUVs are comprised of synthetic
173 lipids which does not reflect the composition of organelle (cilia or ER) membranes of the cell[47]. Thus,
174 while retaining the native ion selectivity and ion channel functionality despite their cell-free origin,
175 synthetic PKD2 has different conductance magnitudes compared to cell derived channels, which
176 presents a limitation of using this approach to recapitulating physiological channel functions.
177 In summary, we have established a synthetic approach to assay ion channel biophysics using two
178 polycystin members to validate our method. Previously CFE has been used to study membrane protein
179 integration, drug delivery, and the study of actin dynamics[29, 48, 49]. The novelty of our approach rests with
180 the adaptation CFE derived channels and their GUV reconstitution to carry out single channel
181 electrophysiology experiments. The described method represents a highly reductionist approach to
182 assay channel function which can be generalized other channels resistant to characterization using
183 traditional electrophysiology approaches. Furthermore, the CFE-GUV electrophysiology method can be
184 leveraged for future inquiry into lipid-channel regulation; effects of channel subunit composition; and
185 ion channel pharmacology.
186
187 **METHODS**
188 *Protein production*
189 Cell-free protein production was performed with PURExpress In Vitro Protein Synthesis Kit from New
190 England Biolabs, Inc. (Ipswich, MA, USA). We utilized the manufacturer's protocol with 1 mg target DNA
191 and a maximum reaction volume of 30 µl. When appropriate, we added substituted DiH2O for SUVs. The

192 reactions were placed in 37°C water bath or heated plate reader between 2 – 3 hours and then placed
193 in 4°C for storage.
194
195 *Vesicle formation*
196 Lipids 1,2-diphytanoyl-sn-glycero-phosphocholine (DPhPC 4ME16:0PC) and cholesterol (ovine) were
197 obtained from Avanti Polar Lipids (Alabaster, AL, USA) and mixed in chloroform to the desired mole
198 percentage, 95% DPhPC and 5% cholesterol. SUVs were formed following the previously described [25].
199 Briefly, lipids were reconstituted in chloroform in a glass vial and the chloroform was evaporated until a
200 thin lipid layer is deposited on the bottom of the glass vial. The lipid layer is then placed under vacuum,
201 -23 inhg, for >4 hours. Lipids are then rehydrated in 1ml of diH2O overnight at 60°C. The following day,
202 lipids are vortexed and then passed through a 100 nm polycarbonate filter with the Mini-Extruder (Avanti
203 Polar Lipids, Alabaster, AL USA) 7 times and stored at 4°C for two weeks. SUVs with or without channel
204 incorporated are dried onto indium tin oxide coated glass slides from Nanion Technologies (Munich,
205 Germany). The dried slides are placed on the Vesicle Prep Pro (Nanion Technologies) with a rubber o-
206 ring and 300 mM sucrose. GUVs are formed using the standard program. Upon GUV formation, vesicles
207 are used same day.
208
209 *Monitoring fluorescence and cell free protein synthesis quantification*
210 We monitored fluorescent folding with PKD2L1 c-terminally tagged GFP during PURExpress reaction in
211 the presence and absence of SUVs. GFP fluorescence was monitored every 10 minutes for three hours
212 at 37°C on the BioTek Cytation5 Imaging Reader (Agilent, Santa Clara, CA, USA). Control plasmid was the
213 PURExpress Control DHFR Plasmid (NEB, Ipswich, MA USA) with no fluorescent tag. Green fluorescent
214 protein (GFP) standard curve was created from dilutions of Aequorea Victoria GFP His-tag recombinant
215 protein (ThermoFisher Scientific, Cat. No. A42613) and measured on the BioTek Cytation5 Imaging
216 Reader. A linear regression (Igor Pro, WaveMetrics, Portland, Or.) was used to create a standard curve.
217 Target protein fluorescent measurements were made after in vitro protein synthesis for three hours.
218
219 *Western blot*
220 Western blotting was performed on PKD2L1–GFP plasmid after PURExpress protein expression in the
221 presence of SUVs. SUV and protein mixture were separated on SDS-PAGE gel, Novex Tris-Glycine mini
222 protein gels, 4-20%, 1.0 mm, WedgeWell format, (ThermoFisher, Waltham, Ma USA). The SDS-PAGE was
223 run with 10 µl Spectra Multicolor Broad Range Protein Ladder (ThermoFisher Scientific, Cat. No. 26634).
224 The gel was then transferred to Amersham Hybond P 0.45 PVDF blotting membrane (Cytiva, Cat. No.
225 10600029) and PKD2L1-GFP was detected with an anti eGFP monoclonal antibody (F56-6A1.2.3)
226 (Invitrogen, Cat. No. MA1-952) diluted 1:1000 in TBS with 0.1% (v/v) Tween-20 and 5% (5/v) milk
227 overnight at 4°C. The goat anti-mouse AF555 secondary (Invitrogen, Cat. No. A32727) diluted 1:5000 in
228 TBS with 0.1% Tween-20 and 5% milk was incubated for 1 hour at room temperature.
229
230 *SNAP staining*

Channel orientation was visualized with n-terminally tagged PKD2L1 with SNAP Tag sequence, (NEB, Ipswich, MA USA). After PKD2L1-SNAP-tag production and incorporation into GUVs, two SPAP-tag substrates were added to the solution, cell permeable SNAP-Cell Oregon Green and the cell impermeable SNAP-Surface Alexa Fluor 647, according to manufacturer's instructions. Images were collected on Nikon A1 confocal microscope and all images were analyzed with Nikon Elements (Melville, N USA). Briefly, regions of interests were manually outlined around the vesicle membrane. Then Pearson's correlation coefficients were measured for fluorescence overlap of the two substrates.

Mammalian culture

HEK 293T cells were authenticated by supplier, ATCC (Manassas, VA USA) and were transiently transfected with jetPRIME transfection reagent, (Axil Scientific Pte Ltd, Singapore), with mammalian cell expression vector pTracer PKD2L1 with IRES GFP. Transfected cells were seeded onto glass coverslips and placed in a recording chamber for cell-attached electrophysiology recordings.

Electrophysiology

All research chemicals were purchased for the electrophysiology experiments from Millipore-Sigma. Single-channel recordings were recorded from primary cilia and GUV membranes. All GUV patch electrodes were made using borosilicate glass electrodes and were fire polished to resistances greater than 5 - 10 MΩ and primary cilia patch electrodes were polished to a resistance greater than 18 MΩ. Recording solutions for mammalian culture consisted of symmetrical recording solutions with 150 mM KCl, 10 mM HEPES, and 300 mM glucose, unless the charge carrier was changed when mentioned. Recordings were collected in voltage-clamp with voltage-steps from -100 mV to +100 mV and a holding potential of -40 mV with ClampEx v.11.2.0.59 (MolecularDevices, San Jose, CA USA) using a Axopatch 200B amplifier. Recordings were digitized with the Digidata 1550B (MolecularDevices) at 25kHz and low pass filtered at 5kHz. Recordings were analyzed with ClampFit v11.2.0.59 (Molecular Devices, San Jose, CA USA) and IGOR Pro 8.04 (Wavemetrics, Portland, OR USA). Conductance was determined by determining the slope of the current-voltage relationship. Probability open time was calculated by measuring the time at which a channel spends in an open confirmation divided by the total time in the voltage step.

ACKNOWLEDGEMENTS

We acknowledge members of the Kamat and DeCaen labs for their constructive comments during the drafting of this manuscript. We thank Dr Alfred George for the use of his lipid electroformation equipment used to generate SUVs and GUVs. M.L was supported by Northwestern University's (NU) molecular biophysics training grant (T32 GM008382) and the National Institute of Diabetes and Digestive and Kidney Diseases (NIDDK) of the National Institutes of Health kidney, urologic and hematologic (KUH) disease training grant (U2CDK129917). O.E.P. was supported by the Ruth L. Kirschstein National Research Service Award (NRSA) individual postdoctoral fellowship (F32DK137477-01A1) and NU KUH training grants (U2CDK129917 and TL1DK132769); P.G.D. was supported by the NIH NIDDK grants R01 DK123463-01 and R01 DK131118-01.

FIGURE LEGENDS

Figure 1. Cell-free expression of synthetic PKD2L1 protein and incorporation into lipid vesicles. A) Schematic of cell-free protein expression into synthetic lipid vesicles and subsequent electroformation with Vesicle Prep Pro (Nanion). **B)** Monitored fluorescence over time of cell-free expressed PKD2L1-GFP and a non-fluorescent control plasmid produced in the presence or absence of lipid vesicles. **C**) Full length PKD2L1-GFP protein detected by Western Blot after cell-free expression into vesicles.

Figure 2. Orientation of synthetic PKD2L1 channels in vesicles. A) Schematic of possible ion channel orientation outcomes from PKD2L1 cell-free expression (top) and hypothesized fluorescence results when Cell488 and Surface647 added (bottom). **B**) Fluorescent confocal images from the SNAP-tagged vesicles. Scale bar represents 10 µm for all images. **C**) Vesicle percentage depicts percent of vesicles with each fluorescent output, (N=65).

Figure 3. Synthetic PKD2L1 channels are functional in artificial membranes. A) Images of voltage clamped GUVs with incorporated PKD2L1-GFP channels. *Left*, establishing high-resistance seals in the on-cell patch configuration. *Right*, transitioning to the inside-our patch configuration. Scale bar = 20 µm. **B**) Example unitary single channel current records from GUVs reconstituted with or without PKD2L1 protein. Vesicles were patched using the symmetrical 150 mM K^+ conditions (see methods) and PKD2L1 single channel current producing full and sub-conductances are colored black and blue, respectively. **C**) Average single-channel current amplitudes. Conductance (γ) estimated by fitting the average single channel currents to a linear equation. Error (grey) indicate SEM from N=2-8 GUVs. Several replicates lacked single channel openings at all test potentials. Conductance estimates from individual GUVs are shown in Figure 3—Supplement Figure 1A. **D**) PKD2L1 single channel current recorded using asymmetric cationic solutions, with 150 mM K^+ in the bath and 150 mM $NMDG^+$ in the pipette. **E**) Resulting average single-channel current amplitudes where no inward single channel current was detected (N=1-4 GUVs).

Figure 4. Functional synthetic PKD2 channels in artificial membranes. A) Example unitary single channel current records from GUVs reconstituted with PKD2 protein in symmetrical 150 mM K^+ conditions producing full (black traces) and sub-conductances (blue traces), respectively. **B**, **C**) Average single-channel current amplitudes recorded using K^+ or $NMDG^+$ in the recording electrode solution. Conductance (γ) estimated by fitting the average single channel currents to a linear equation. Error (grey) indicate SEM from K^+ (N=2-12 GUVs) and $NMDG^+$ (N=1-5 GUVs) conditions.

Table 1. Conductance properties of polycystins measured from GUV and cilia membranes.

Figure 1— figure supplement 1. Quantification and identification of cell-free synthesized PKD2L1 channel protein. A). *Left*, Fluorescence (488γ) standard curve determined with a recombinant GFP tagged protein fit with a linear regression. PURExpress synthesized PKD2L1-GFP and PKD2-GFP were measured after three hours of expression at 37°C. (GFP standard curve N=5, PKD2L1 and PKD2 N=3).

311 *Right*, average protomer and tetramer protein production from the PURExpress reaction. Error bars
312 represent SEM. **B**) Representative sequence coverage of PKD2L1-GFP (top) and PKD2-GFP (bottom) from
313 tandem mass spectrometry spectra. **C**) Mass spectrometry outputs identifying polycystin proteins.
314
315 **Figure 2— figure supplement 1. The SNAP- fluorescence approach to assess polycystin protein**
316 **orientation in GUV**. Schematic of PKD2L1-SNAP incorporated into GUVs, followed by SNAP-staining with
317 cell permeable (Cell488), and cell impermeable (Surface647) SNAP-Tag marker.
318
319 **Figure 3—figure supplement 1. Synthetic polycystin channels exhibit full and sub-conductive states in**
320 **GUVs. A, E)** Single channel current amplitudes measured from individual GUVs (open circles). GUVs with
321 open channel events measure at four or more potentials in inward and outward direction were fit to a
322 linear equation to estimate their conductance. **B, F)** Resulting violin plots of the sub (*SC*, blue) and full
323 (*FC*, black) polycystin conductance as estimated from individual GUV recordings. **C, G)** Unitary single
324 channel currents measured from GUVs expressing polycystins held at 100 mV. Examples on the top
325 demonstrated channels transitioning from closed (*C*) to the full conductance current levels, whereas
326 examples below are measured from channels shifting between sub- and fully conductive current levels.
327 **D, H**) Resulting histogram analysis of the corresponding single channel currents.
328
329 **Figure 4—figure supplement 1 . Native polycystin channels measured from primary cilia membranes**
330 **exhibit full and subconductance states. A**, **B**) *Top*, images of voltage clamped primary cilia from mouse
331 hippocampal neurons and inner medullary kidney collecting duct cells (IMCD) harvested from transgenic
332 mice expressing a fluorescent cilia reporter (ARL13B-EGFP^{tg})[50]. Previous work has genetically identified
333 PKD2L1 and PKD2 as essential ion channel subunit in the primary cilia of the renal collecting duct cells
334 and hippocampal neurons[34, 42]. *Bottom*, average single-channel current amplitudes recorded from
335 primary cilia using K^+ in the recording electrode solution. Conductance (γ) estimated by fitting the
336 average single channel currents to a linear equation. Error indicates SEM (N=6 cilia).
337
338 **REFERENCES**

339 1. Hille, B., Ionic channels in excitable membranes. Current problems and biophysical approaches.
340 *Biophysical journal* **1978,** *22* (2), 283-294.
341 2. Lee, A.; Fakler, B.; Kaczmarek, L. K.; Isom, L. L., More than a pore: ion channel signaling complexes. *J*
342 *Neurosci* **2014,** *34* (46), 15159-15169.
343 3. Yang, Y.; Wang, Z.; Gan, C.; Klausen, L. H.; Bonne, R.; Kong, G.; Luo, D.; Meert, M.; Zhu, C.; Sun, G.;
344 Guo, J.; Ma, Y.; Bjerg, J. T.; Manca, J.; Xu, M.; Nielsen, L. P.; Dong, M., Long-distance electron transfer in a
345 filamentous Gram-positive bacterium. *Nat Commun* **2021,** *12* (1), 1709.
346 4. Prindle, A.; Liu, J.; Asally, M.; Ly, S.; Garcia-Ojalvo, J.; Suel, G. M., Ion channels enable electrical
347 communication in bacterial communities. *Nature* **2015,** *527* (7576), 59-63.
348 5. Goaillard, J. M.; Marder, E., Ion Channel Degeneracy, Variability, and Covariation in Neuron and Circuit
349 Resilience. *Annu Rev Neurosci* **2021,** *44*, 335-357.
350 6. Stutzmann, G. E.; Mattson, M. P., Endoplasmic reticulum Ca(2+) handling in excitable cells in health and
351 disease. *Pharmacol Rev* **2011,** *63* (3), 700-27.
352 7. Smith, J. J.; Aitchison, J. D., Peroxisomes take shape. *Nat Rev Mol Cell Biol* **2013,** *14* (12), 803-17.

8. Li, P.; Gu, M.; Xu, H., Lysosomal Ion Channels as Decoders of Cellular Signals. *Trends Biochem Sci* **2019,** *44* (2), 110-124.
9. Yu, F. H.; Yarov-Yarovoy, V.; Gutman, G. A.; Catterall, W. A., Overview of molecular relationships in the voltage-gated ion channel superfamily. *Pharmacol Rev* **2005,** *57* (4), 387-95.
10. George, A. L., Jr., Lessons learned from genetic testing for channelopathies. *Lancet Neurol* **2014,** *13* (11), 1068-1070.
11. George, A. L., Jr., Recent genetic discoveries implicating ion channels in human cardiovascular diseases. *Curr Opin Pharmacol* **2014,** *15*, 47-52.
12. Clare, J. J., Targeting voltage-gated sodium channels for pain therapy. *Expert Opin Investig Drugs* **2010,** *19* (1), 45-62.
13. Lieve, K. V.; Wilde, A. A., Inherited ion channel diseases: a brief review. *Europace* **2015,** *17 Suppl 2*, ii1-6.
14. Kass, R. S., The channelopathies: novel insights into molecular and genetic mechanisms of human disease. *J Clin Invest* **2005,** *115* (8), 1986-9.
15. Overington, J. P.; Al-Lazikani, B.; Hopkins, A. L., How many drug targets are there? *Nat Rev Drug Discov* **2006,** *5* (12), 993-6.
16. Santos, R.; Ursu, O.; Gaulton, A.; Bento, A. P.; Donadi, R. S.; Bologa, C. G.; Karlsson, A.; Al-Lazikani, B.; Hersey, A.; Oprea, T. I.; Overington, J. P., A comprehensive map of molecular drug targets. *Nat Rev Drug Discov* **2017,** *16* (1), 19-34.
17. Kaczorowski, G. J.; McManus, O. B.; Priest, B. T.; Garcia, M. L., Ion channels as drug targets: the next GPCRs. *J Gen Physiol* **2008,** *131* (5), 399-405.
18. Oprea, T. I., Exploring the dark genome: implications for precision medicine. *Mamm Genome* **2019,** *30* (7-8), 192-200.
19. McGivern, J. G.; Ding, M., Ion Channels and Relevant Drug Screening Approaches. *SLAS Discov* **2020,** *25* (5), 413-419.
20. Neher, E.; Sakmann, B., Single-channel currents recorded from membrane of denervated frog muscle fibres. *Nature* **1976,** *260* (5554), 799-802.
21. Neher, E., Ion channels for communication between and within cells. *Science* **1992,** *256* (5056), 498-502.
22. Hamill, O. P.; Marty, A.; Neher, E.; Sakmann, B.; Sigworth, F. J., Improved patch-clamp techniques for high-resolution current recording from cells and cell-free membrane patches. *Pflugers Arch* **1981,** *391* (2), 85-100.
23. Morera, F. J.; Vargas, G.; Gonzalez, C.; Rosenmann, E.; Latorre, R., Ion-channel reconstitution. *Methods Mol Biol* **2007,** *400*, 571-85.
24. Leptihn, S.; Thompson, J. R.; Ellory, J. C.; Tucker, S. J.; Wallace, M. I., In vitro reconstitution of eukaryotic ion channels using droplet interface bilayers. *J Am Chem Soc* **2011,** *133* (24), 9370-5.
25. Varghese, A.; Tenbroek, E. M.; Coles, J., Jr.; Sigg, D. C., Endogenous channels in HEK cells and potential roles in HCN ionic current measurements. *Prog Biophys Mol Biol* **2006,** *90* (1-3), 26-37.
26. Pablo, J. L.; DeCaen, P. G.; Clapham, D. E., Progress in ciliary ion channel physiology. *J Gen Physiol* **2017,** *149* (1), 37-47.
27. Shimizu, Y.; Ueda, T., PURE technology. *Methods Mol Biol* **2010,** *607*, 11-21.
28. Kuruma, Y.; Nishiyama, K.; Shimizu, Y.; Müller, M.; Ueda, T., Development of a minimal cell-free translation system for the synthesis of presecretory and integral membrane proteins. *Biotechnol Prog* **2005,** *21* (4), 1243-51.
29. Jacobs, M. L.; Kamat, N. P., Cell-Free Membrane Protein Expression into Hybrid Lipid/Polymer Vesicles. *Methods Mol Biol* **2022,** *2433*, 257-271.
30. Esarte Palomero, O.; Larmore, M.; DeCaen, P. G., Polycystin Channel Complexes. *Annu Rev Physiol* **2023,** *85*, 425-448.
31. Wu, G.; D'Agati, V.; Cai, Y.; Markowitz, G.; Park, J. H.; Reynolds, D. M.; Maeda, Y.; Le, T. C.; Hou, H., Jr.; Kucherlapati, R.; Edelmann, W.; Somlo, S., Somatic inactivation of Pkd2 results in polycystic kidney disease. *Cell* **1998,** *93* (2), 177-88.

400 32. Gao, Z.; Ruden, D. M.; Lu, X., PKD2 cation channel is required for directional sperm movement and male
401 fertility. *Curr Biol* **2003,** *13* (24), 2175-8.
402 33. Tanaka, Y.; Morozumi, A.; Hirokawa, N., Nodal flow transfers polycystin to determine mouse left-right
403 asymmetry. *Dev Cell* **2023,** *58* (16), 1447-1461 e6.
404 34. Vien, T. N.; Ta, M. C.; Kimura, L. F.; Onay, T.; DeCaen, P. G., Primary cilia TRP channel regulates hippocampal
405 excitability. *Proc Natl Acad Sci U S A* **2023,** *120* (22), e2219686120.
406 35. Yao, G.; Luo, C.; Harvey, M.; Wu, M.; Schreiber, T. H.; Du, Y.; Basora, N.; Su, X.; Contreras, D.; Zhou, J.,
407 Disruption of polycystin-L causes hippocampal and thalamocortical hyperexcitability. *Hum Mol Genet* **2016,** *25* (3),
408 448-58.
409 36. Vo, C. V.; Mikutis, G.; Bode, J. W., SnAP reagents for the transformation of aldehydes into substituted
410 thiomorpholines--an alternative to cross-coupling with saturated heterocycles. *Angew Chem Int Ed Engl* **2013,** *52*
411 (6), 1705-8.
412 37. Müller-Lucks, A.; Bock, S.; Wu, B.; Beitz, E., Fluorescent in situ folding control for rapid optimization of
413 cell-free membrane protein synthesis. *PLoS One* **2012,** *7* (7), e42186.
414 38. Klammt, C.; Schwarz, D.; Löhr, F.; Schneider, B.; Dötsch, V.; Bernhard, F., Cell-free expression as an
415 emerging technique for the large scale production of integral membrane protein. *Febs j* **2006,** *273* (18), 4141-53.
416 39. Boban, Z.; Mardesic, I.; Subczynski, W. K.; Raguz, M., Giant Unilamellar Vesicle Electroformation: What to
417 Use, What to Avoid, and How to Quantify the Results. *Membranes (Basel)* **2021,** *11* (11).
418 40. DeCaen, P. G.; Liu, X.; Abiria, S.; Clapham, D. E., Atypical calcium regulation of the PKD2-L1 polycystin ion
419 channel. *Elife* **2016,** *5*.
420 41. Ng, L. C. T.; Vien, T. N.; Yarov-Yarovoy, V.; DeCaen, P. G., Opening TRPP2 (PKD2L1) requires the transfer of
421 gating charges. *Proc Natl Acad Sci U S A* **2019,** *116* (31), 15540-15549.
422 42. Kleene, S. J.; Kleene, N. K., The native TRPP2-dependent channel of murine renal primary cilia. *Am J Physiol*
423 *Renal Physiol* **2017,** *312* (1), F96-F108.
424 43. Liu, X.; Vien, T.; Duan, J.; Sheu, S. H.; DeCaen, P. G.; Clapham, D. E., Polycystin-2 is an essential ion channel
425 subunit in the primary cilium of the renal collecting duct epithelium. *Elife* **2018,** *7*.
426 44. Cai, Y.; Maeda, Y.; Cedzich, A.; Torres, V. E.; Wu, G.; Hayashi, T.; Mochizuki, T.; Park, J. H.; Witzgall, R.;
427 Somlo, S., Identification and characterization of polycystin-2, the PKD2 gene product. *J Biol Chem* **1999,** *274* (40),
428 28557-65.
429 45. Newby, L. J.; Streets, A. J.; Zhao, Y.; Harris, P. C.; Ward, C. J.; Ong, A. C., Identification, characterization,
430 and localization of a novel kidney polycystin-1-polycystin-2 complex. *J Biol Chem* **2002,** *277* (23), 20763-73.
431 46. Su, Q.; Hu, F.; Liu, Y.; Ge, X.; Mei, C.; Yu, S.; Shen, A.; Zhou, Q.; Yan, C.; Lei, J.; Zhang, Y.; Liu, X.; Wang,
432 T., Cryo-EM structure of the polycystic kidney disease-like channel PKD2L1. *Nat Commun* **2018,** *9* (1), 1192.
433 47. Nakatsu, F., A Phosphoinositide Code for Primary Cilia. *Dev Cell* **2015,** *34* (4), 379-80.
434 48. Noireaux, V.; Liu, A. P., The New Age of Cell-Free Biology. *Annu Rev Biomed Eng* **2020,** *22*, 51-77.
435 49. Gopfrich, K.; Haller, B.; Staufer, O.; Dreher, Y.; Mersdorf, U.; Platzman, I.; Spatz, J. P., One-Pot Assembly
436 of Complex Giant Unilamellar Vesicle-Based Synthetic Cells. *ACS Synth Biol* **2019,** *8* (5), 937-947.
437 50. Delling, M.; DeCaen, P. G.; Doerner, J. F.; Febvay, S.; Clapham, D. E., Primary cilia are specialized calcium
438 signalling organelles. *Nature* **2013,** *504* (7479), 311-4.

439

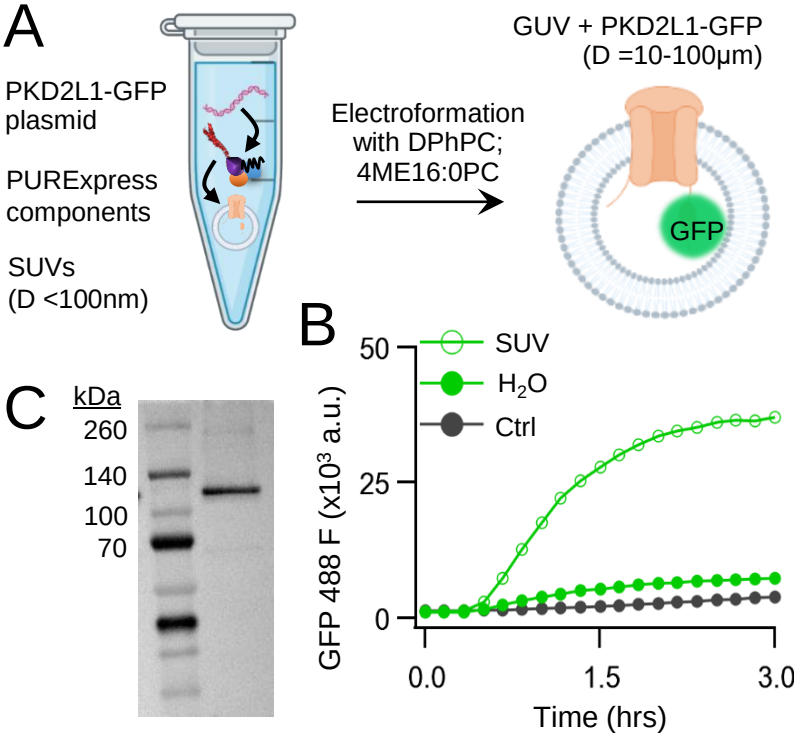
A
PKD2L1-GFP plasmid
PURExpress components
SUVs (D <100nm)
Electroformation with DPhPC; 4ME16:0PC
GUV + PKD2L1-GFP (D =10-100µm)
GFP
B
SUV
H2O
Ctrl
GFP 488 F (x10^3 a.u.)
50
25
0
0.0
1.5
3.0
Time (hrs)
C
kDa
260
140
100
70

Figure 1

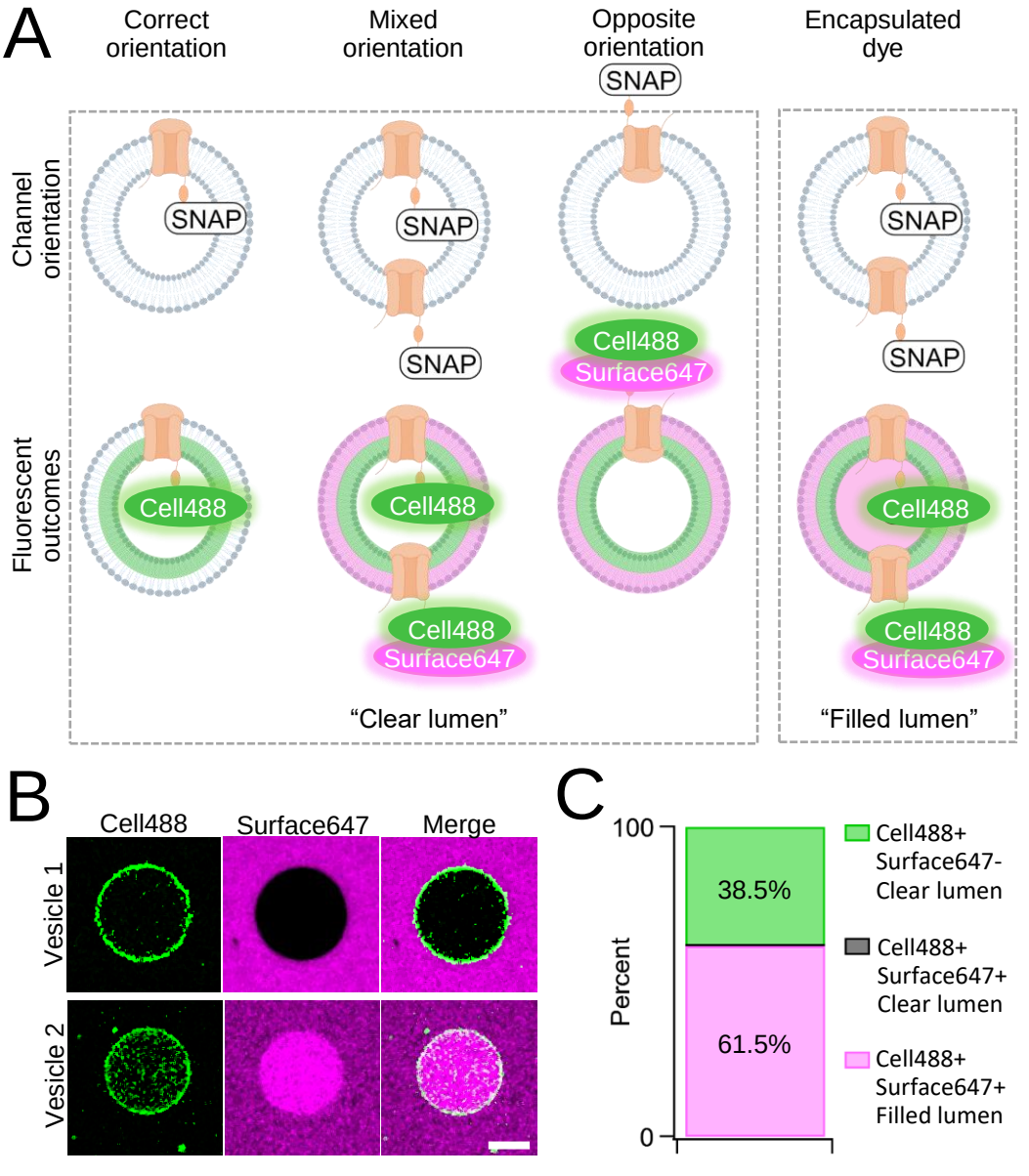
A
Correct orientation
Mixed orientation
Opposite orientation
Encapsulated dye
Channel orientation
Fluorescent outcomes
SNAP
Cell488
Surface647
"Clear lumen"
"Filled lumen"
B
Cell488
Surface647
Merge
Vesicle 1
Vesicle 2
C
100
0
Percent
38.5%
61.5%
Cell488+ Surface647- Clear lumen
Cell488+ Surface647+ Clear lumen
Cell488+ Surface647+ Filled lumen

Figure 2

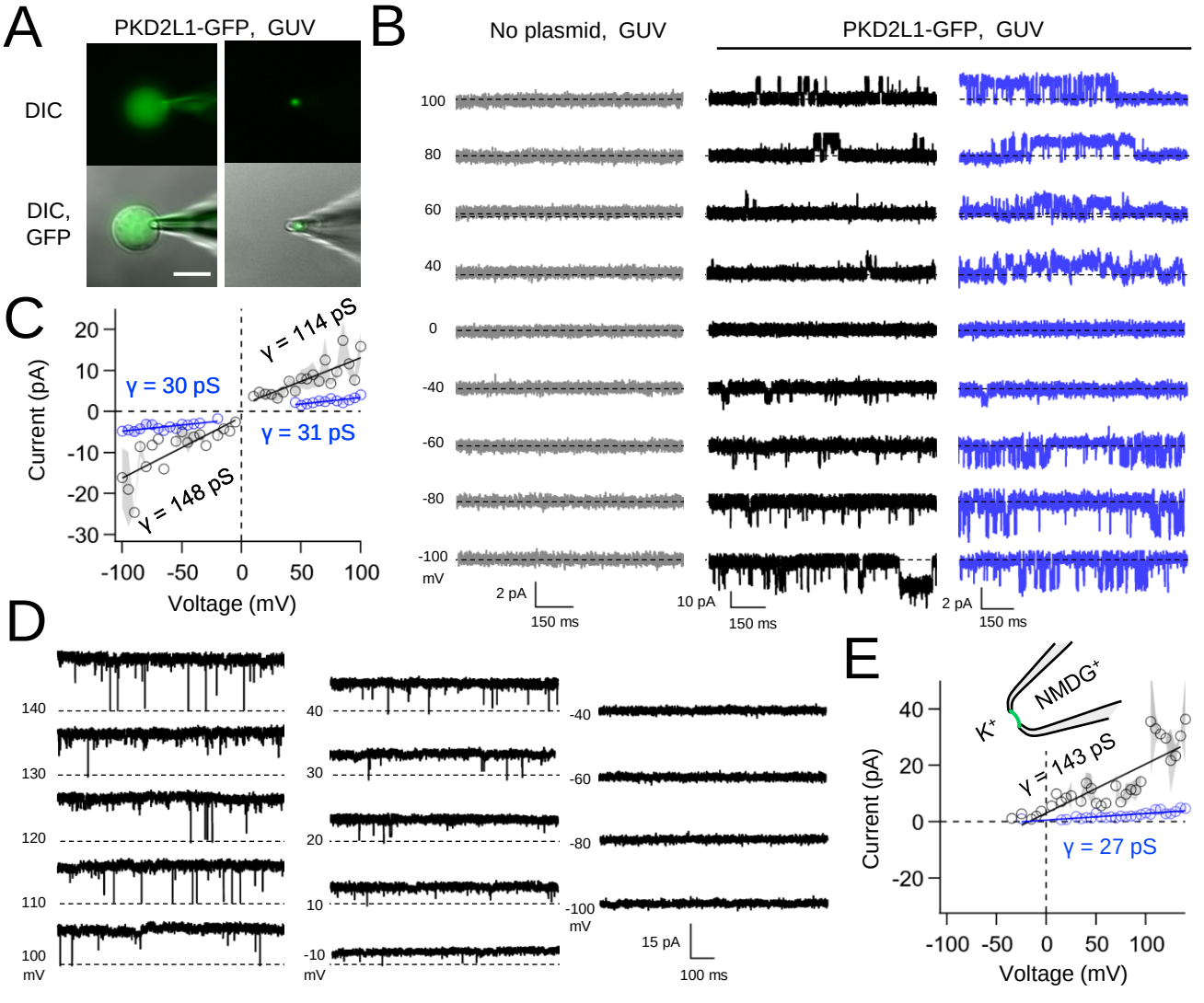
A
PKD2L1-GFP, GUV
DIC
DIC, GFP
B
No plasmid, GUV
PKD2L1-GFP, GUV
100
80
60
40
0
-40
-60
-80
-100
mV
2 pA
150 ms
10 pA
150 ms
2 pA
150 ms
C
γ = 114 pS
γ = 30 pS
γ = 31 pS
γ = 148 pS
Current (pA)
Voltage (mV)
D
140
130
120
110
100
mV
40
30
20
10
-10
mV
-40
-60
-80
-100
mV
15 pA
100 ms
E
NMDG+
K+
γ = 143 pS
γ = 27 pS
Current (pA)
Voltage (mV)

Figure 3

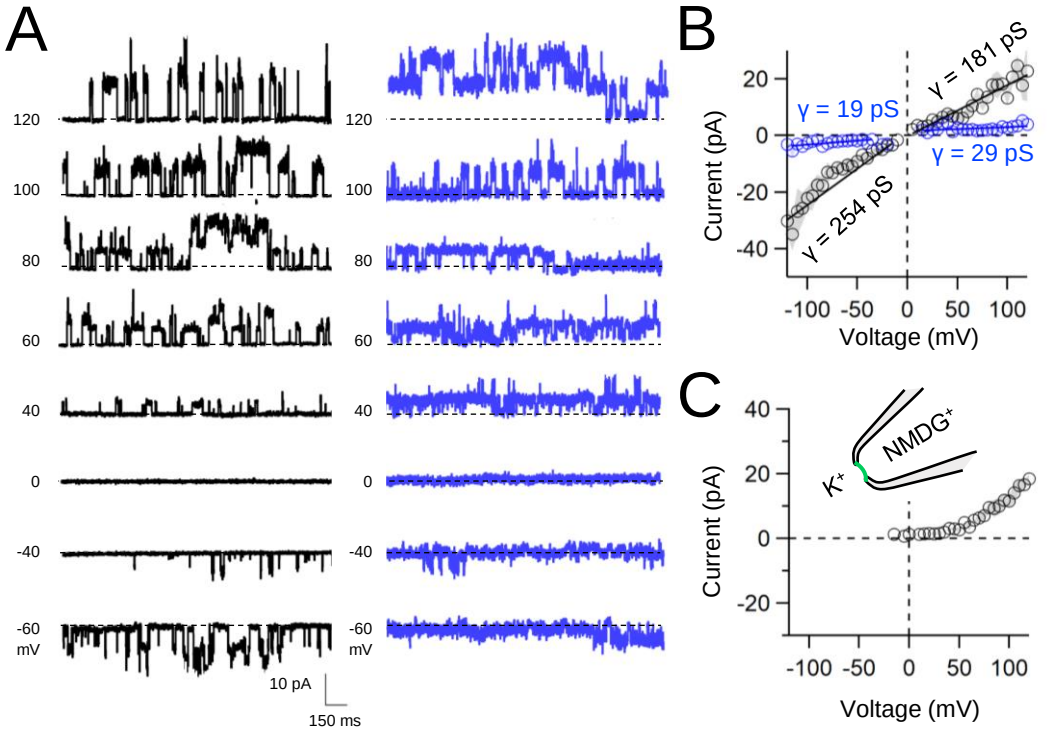
A
120
100
80
60
40
0
-40
-60
mV
10 pA
150 ms
B
γ = 181 pS
γ = 19 pS
γ = 29 pS
γ = 254 pS
Current (pA)
Voltage (mV)
C
K+
NMDG+
Current (pA)
Voltage (mV)

Figure 4

A

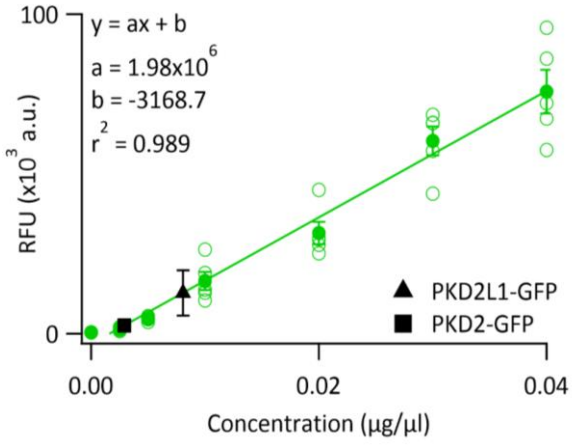

	Average protomer [ng/ul]	Average tetramer [ng/ul]
PKD2L1	8.0 ± 3.6	2.0 ± 0.9
PKD2	3.1 ± 2	0.8 ± 0.07

B

Peptide coverage

PKD2L1-GFP

MNAVGSPEGQELQKLGSGAWDNPAYSGPPSPHGTLRVCTISSTGPLQPQPKKPEDEPQETAYRTQVSSCCLHICQGIRGLW
GTTLTENTAENRELYIKTTLRELLVYIVFLVDICLLTYGMTSSSAYYYTKVMSELFLHTPSDTGVSFQAISSMADFWDFAQGPL
LDSLYWTKWYNNQSLGHGSHSFIYYENMLLGVPRLRQLKVRNDSCVVHEDFREDILSCYDVYSPDKEEQLPFGPFNGTAWT
YHSQDELGGFSHWGRLTSYSGGGYYLDLPGSRQGSAEALRALQEGLWLDRGTRVVFIDFSVYNANINLFCVLRLVVEFPATG
GAIPSWQIRTVKLIRYVSNWDFFIVGCEVIFCVFIFYYVVEEILELHIHRLRYLSSIWNILDLVVILLSIVAVGFHIFRTLEVNRL
MGKLLQQPNTYADFEFLAFWQTQYNNMNAVNLFFAWIKIFKYISFNKTMTQLSSTLARCAKDILGFAVMFFIVFFAYAQLGYL
LFGTQVENFSTFIKCIFTQFRIILGDFDYNAIDNANRILGPAYFVTYVFFVFFVLLNMFLAIINDTYSEVKEELAGQKDELQLSD
LLKQGYNKTLLRLRLRKERVSDVQKVLQGGEQEIQFEDFTNTLRELGHAEHEITELTATFTKFDRDGNRILDEKEQEKMRQDL
EEERVALNTEIEKLGRSIVSSPQGKSGPEAARAGGWVSGEEFYMLTRRVLQLETVLEGVVSQIDAVGSKLKMLERKGWLAPS
PGVKEQAIWKHPQPAPAVTPDPWGVQGGQESEVPYKREEEALEERRLSRGEIPTLQRSMSKGEELFTGVVPILVELDGDVN
GHKFSVSGEGEGDATYGKLTLKFICTTGKLPVPWPTLVTTFSYGVQCFSRYPDHMKQHDFFKSAMPEGYVQERTIFFKDDGN
YKTRAEVKFEGDTLVNRIELKGIDFKEDGNILGHKLEYNYNSHNVYIMADKQKNGIKVNFKIRHNIEDGSVQLADHYQQNTPI
GDGPVLLPDNHYLSTQSALSKDPNEKRDHMVLLEFVTAAGITHGMDELYK

PKD2-GFP

MVNSSRVQPQQPGDAKRPPAPRAPDPGRLMAGCAAVGASLAAPGGLCEQRGLEIEMQRIRQAAARDPPAGAAASPSPPLSSCSRQAW
SRDNPGFEAEEEEEEVEGEEGGMVVEMDVEWRPGSRRSAASSAVSSVGARSRGLGGYHGAGHPSGRRRRREDQGPPCPSPVGGGD
PLHRHLPLEGQPPRVAWAERLVRGLRGLWGTRLMEESSTNREKYLKSVLRELVTYLLFLIVLCILTYGMMSSNVYYYTRMMSQLFLDTP
VSKTEKTNFKTLSSMEDFWKFTEGSLLDGLYWKMQPSNQTEADNRSFIFYENLLLGVPRIRQLRVRNGSCSIPQDLRDEIKECYDVYSV
SSEDRAPFGPRNGTAWIYTSEKDLNGSSHWGIIATYSGAGYYLDLSRTREETAAQVASLKKNVWLDRGTRATFIDFSVYNANINLFCVV
RLLVEFPATGGVIPSWQFQPLKLIRYVTTFDFFLAACEIIFCFFIFYYVVEEILEIRIHKLHYFRSFWNCLDVVIVVLSVVAIGINIYRTSNVE
VLLQFLEDQNTFPNFEHLAYWQIQFNNIAAVTVFFVWIKLFKFINFNRTMSQLSTTMSRCAKDLFGFAIMFFIIFLAYAQLAYLVFGTQVD
DFSTFQECIFTQFRIILGDINFAEIEEANRVLGPIYFTTFVFFMFFILLNMFLAIINDTYSEVKSDLAQQKAEMELSDLIRKGYHKALVKLKL
KKNTVDDISESLRQGGGKLNFDELRQDLKGKGHTDAEIEAIFTKYDQDGDQELTEHEHQQMRDDLEKEREDLDLDHSSLPRPMSSRSF
PRSLDDSEEDDDEDSGHSSRRRGSISSGVSYEEFQVLVRRVDRMEHSIGSIVSKIDAVIVKLEIMERAKLKRREVLGRLLDGVAEDERL
GRDSEIHREQMERLVREELERWESDDAASQISHGLGTPVGLNGQPRPRSSRPSSSQSTEGMEGAGGNGSSNVHVMSKGEELFTGVVP
ILVELDGDVNGHKFSVSGEGEGDATYGKLTLKFICTTGKLPVPWPTLVTTFSYGVQCFSRYPDHMKQHDFFKSAMPEGYVQERTIFFKD
DGNYKTRAEVKFEGDTLVNRIELKGIDFKEDGNILGHKLEYNYNSHNVYIMADKQKNGIKVNFKIRHNIEDGSVQLADHYQQNTPIGDGP
VLLPDNHYLSTQSALSKDPNEKRDHMVLLEFVTAAGITHGMDELYK

C

	Protein identification probability	Percent coverage	Exclusive unique peptides
PKD2L1-GFP	100%	46%	22
PKD2-GFP	100%	25%	63

Figure 1—Figure Supplement 1

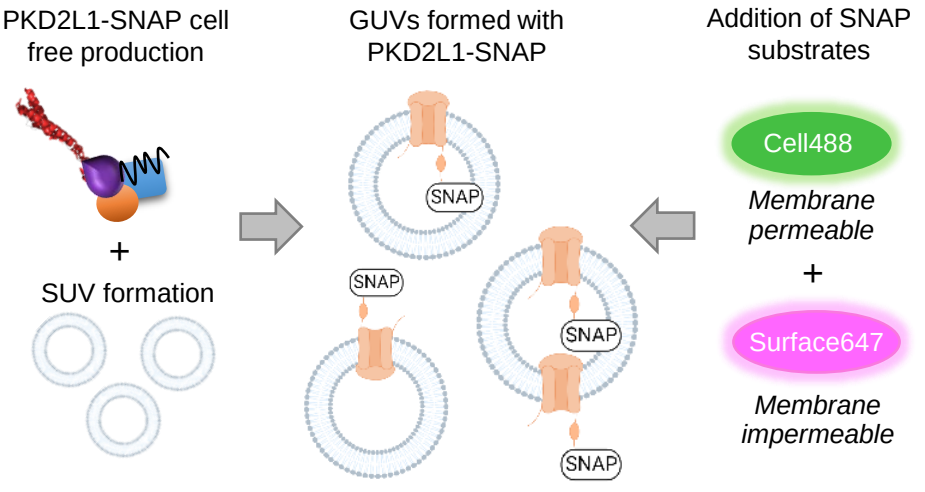

Figure 2– Figure supplement 1

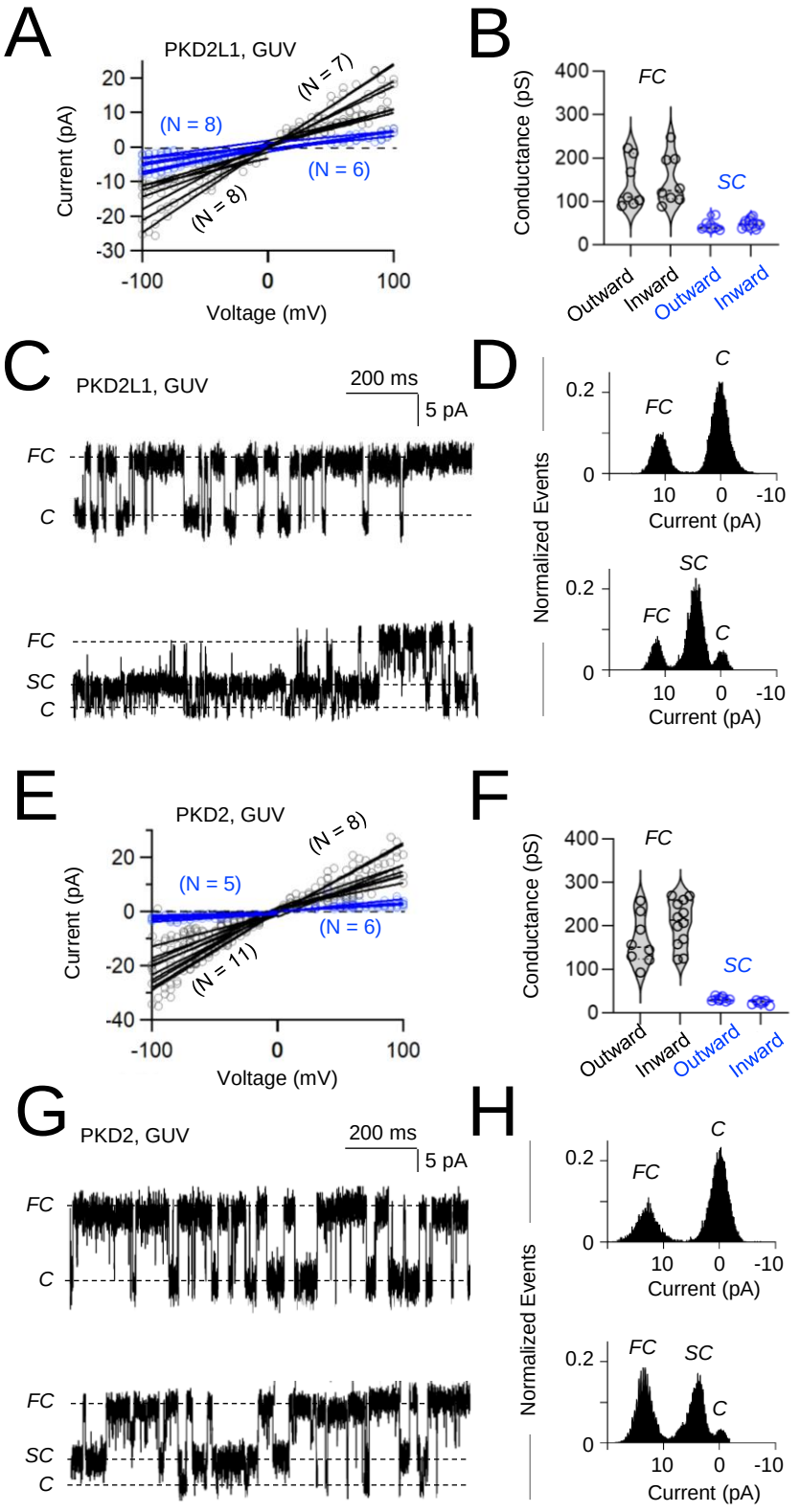

Figure 3– Figure Supplement 1

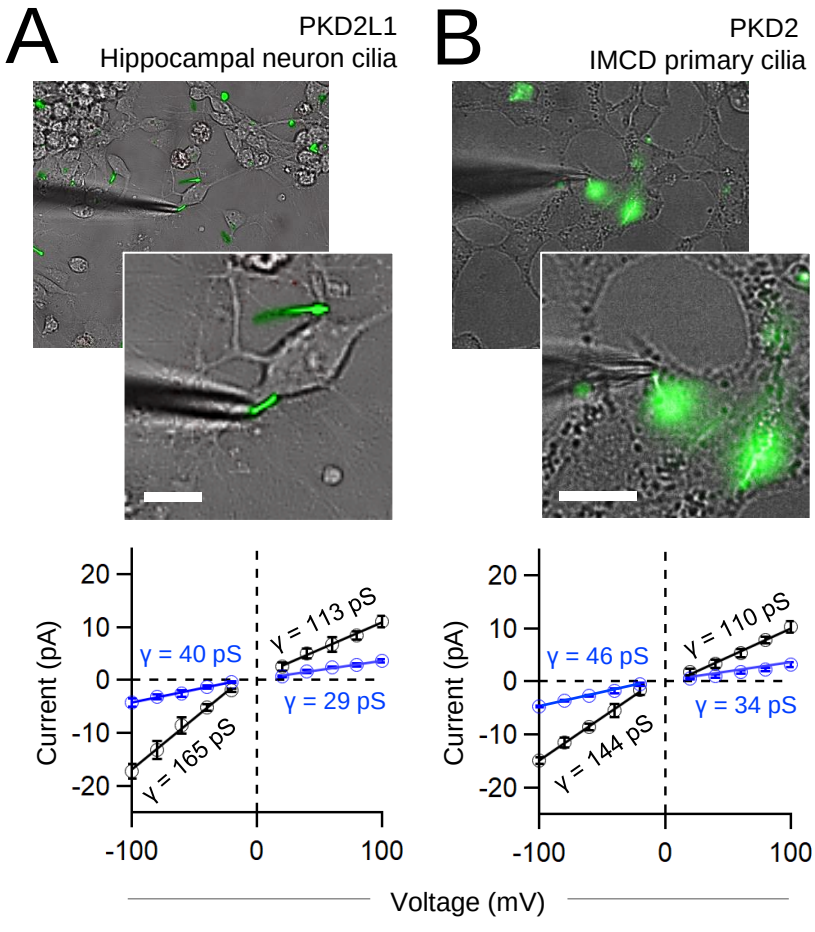

Figure 4– Figure supplement 1

Polycystin channel and membrane context.	**Major K^+ γ (pS) ± S.D.**		**Minor K^+ γ (pS) ± S.D.**	
	inward	*outward*	*inward*	*outward*
PKD2 (GUV membrane, cell free expression)	282 ± 38	153 ± 32	23 ± 4	21 ± 3
PKD2 (primary cilia membrane, endogenous murine IMCD cell line)	144 ± 9	110 ± 6	46 ± 4	34 ± 4
PKD2L1 (GUV membrane, cell free expression)	148 ± 29	114 ± 28	30 ± 6	31 ± 7
PKD2L1 (primary cilia membrane, endogenous hippocampal neurons)	165 ± 10	113 ± 6	40 ± 4	29 ± 3

Table 1